Nie et al. *Zool. Res.* 2025, 46(1): 3−14
https://doi.org/10.24272/j.issn.2095-8137.2024.409
https://cstr.cn/32248.14.zr.2024.409

ZR | Zoological Research

Article Open Access

Palmitoylation-mediated NLRP3 inflammasome activation in teleosts highlights evolutionary divergence in immune regulation

Li Nie[1,2,3,#,*], Xiang-Yu Wu[1,2,3,#], Zi-Yue Zhao[1,2,3], Chen-Jie Fei[1,2,3], Ting-Fang Zhu[1,2,3], Jian-Zhong Shao[4,*], Jiong Chen[1,2,3,*]

[1] *State Key Laboratory for Managing Biotic and Chemical Threats to the Quality and Safety of Agro-Products*, *School of Marine Sciences*, *Ningbo University*, *Ningbo*, *Zhejiang* 315211, *China*

[2] *Laboratory of Biochemistry and Molecular Biology*, *School of Marine Sciences*, *Ningbo University*, *Ningbo*, *Zhejiang* 315211, *China*

[3] *Key Laboratory of Aquaculture Biotechnology of Ministry of Education*, *Ningbo University*, *Ningbo*, *Zhejiang* 315211, *China*

[4] *College of Life Sciences*, *Key Laboratory for Cell and Gene Engineering of Zhejiang Province*, *Zhejiang University*, *Hangzhou*, *Zhejiang* 310058, *China*

ABSTRACT

NLRP3 inflammasome activation is pivotal for cytokine secretion and pyroptosis in response to diverse stimuli, playing a crucial role in innate immunity. While extensively studied in mammals, the regulatory mechanisms governing NLRP3 activation in non-mammalian vertebrates remain largely unexplored. Teleosts, as basal vertebrates, represent an ideal model for exploring the evolutionary trajectory of inflammasome regulation. In this study, ABE assays, confocal microscopy, and biochemical analyses were applied to systematically characterize the mechanisms underlying NLRP3 inflammasome in teleosts, using large yellow croakers (*Larimichthys crocea*, *Lc*) and zebrafish (*Danio rerio*, *Dr*) as representative models. Our findings revealed a previously unrecognized palmitoylation-dependent regulatory mechanism essential for teleost NLRP3 activation. Specifically, zDHHC18-mediated palmitoylation at a teleost-specific cysteine residue (C946 in *Lc*NLRP3, C1037 in *Dr*NLRP3) was required for the translocation of NLRP3 to the dispersed trans-Golgi network, facilitating its subsequent recruitment to the microtubule-organizing center. This membrane trafficking was crucial for inflammasome assembly and downstream inflammatory responses. These findings provide new insights into the distinct regulatory mechanisms of NLRP3 activation in teleosts, highlighting an evolutionary divergence that contributes to innate immunity adaptation in early vertebrates.

Keywords: NLRP3; Palmitoylation; zDHHC18; Teleost; Inflammasome activation

INTRODUCTION

The inflammasome serves as a critical molecular hub for initiating inflammatory responses by activating inflammatory caspases and driving cytokine maturation (Martinon et al., 2002). Among the various inflammasomes identified to date, the NLRP3 inflammasome is the most extensively studied due to its broad involvement in diverse biological processes and its involvement in the pathogenesis of numerous diseases (Holbrook et al., 2021; Mangan et al., 2018; Sharma & Kanneganti, 2021; Tan et al., 2013). The canonical NLRP3 inflammasome is a multi-protein complex composed of the sensor molecule NACHT-, leucine-rich repeat (LRR)- and pyrin domain (PYD)-containing protein 3 (NLRP3), the adaptor protein apoptosis associated speck-like protein containing a CARD (ASC), and the effector protein pro-Caspase-1 (He et al., 2016a). Upon activation, Caspase-1 cleaves the cytokine precursors pro-IL-1β and pro-IL-18 into their mature forms, driving robust inflammatory responses. Concurrently, Caspase-1 cleaves and activates gasdermin D (GSDMD), releasing its N-terminal domain to form plasma membrane-spanning pores, thereby inducing pyroptosis, a lytic and highly inflammatory form of programmed cell death (Franchi et al., 2009; Shi et al., 2015).

Despite its well-established role in innate immunity, our understanding of the regulatory mechanisms governing NLRP3 inflammasome activation is primarily limited to mammalian species, leaving significant gaps in our

Received: 14 November 2024; Accepted: 09 December 2024; Online: 10 December 2024

Foundation items: This work was supported by the National Natural Science Foundation of China (32473194), Natural Science Foundation of Zhejiang Province (LY23C190002), Natural Science Foundation of Ningbo City (202003N4011), and One Health Interdisciplinary Research Project of Ningbo University (HZ202201)

[#]Authors contributed equally to this work

*Corresponding authors, E-mail: nieli@nbu.edu.cn; shaojz@zju.edu.cn; chenjiong@nbu.edu.cn

understanding of its function and evolutionary development in non-mammalian vertebrates. The components, membrane translocation, assembly, and regulation of the NLRP3 inflammasome in non-mammalian vertebrates remain largely unexplored, although the innate immune network in lower vertebrates is considerably more complex than in mammals. Teleosts, positioned at the intersection of innate and adaptive immunity (Boehm & Swann, 2014), provide an ideal model for studying the evolutionary regulation of the NLRP3 inflammasome.

Recent studies underscore the suitability of teleosts for inflammasome research. Key inflammasome components, including NLRP3, ASC, Caspase-1, and GSDME — the sole gasdermin family member associated with pyroptosis in teleosts—have been identified in teleosts in recent years. For instance, in Japanese flounder, NLRP3 inflammasome activation has been shown to play a vital role in restricting *Edwardsiella piscicida* colonization through the maturation of IL-1β, a crucial step in mounting effective host immune responses against bacterial infections (Chen et al., 2020). Similarly, zebrafish studies have demonstrated that the NLRP3 inflammasome coordinates ASC-dependent IL-1β maturation and GSDME-mediated pyroptosis, highlighting its pivotal role in inflammation and cell death (Li et al., 2020b). Unique inflammatory regulatory mechanisms have also been discovered in turbot, where *Sm*Caspase, an inflammatory caspase, mediates both canonical and non-canonical inflammasome pathways. *Sm*Caspase possesses the ability to recognize cytosolic lipopolysaccharides (LPS) via its N-terminal CARD domain, driving pyroptosis and antibacterial defenses (Chen et al., 2021). Moreover, *Sm*Caspase interacts with *Sm*NLRP3-*Sm*ASC to form the NLRP3 inflammasome complex, further emphasizing its multifunctionality in teleost immune responses. Comparative studies on *Salmo salar* and *Tetraodon* have also provided insights into the role of the NLRP3 inflammasome in immune regulation and its evolutionary conservation with mammals (Acevedo et al., 2023). Notably, fish inflammasomes can function independently of caspase-1 for IL-1β processing, as observed in seabream macrophages, indicating the presence of alternative cytokine maturation pathways (Angosto et al., 2012). Furthermore, two distinct models of NLRP3 inflammasome assembly have emerged in teleosts, distinguished by the domain architecture of their Caspase-1 homologs: one involving PYD-containing Caspase-1, as seen in zebrafish, and the other involving CARD-containing Caspase-1, which resembles the mammalian homolog and is found in most teleost species (Chuphal et al., 2022; Li et al., 2020b).

In this study, the large yellow croaker (*Larimichthys crocea*, *Lc*), an economically important marine species endemic to China, was used as a representative CARD-containing Caspase-1 inflammasome model with a well-sequenced genome. Large yellow croakers are highly susceptible to environmental stress and pathogen-induced diseases (Ao et al., 2015; Chen et al., 2019; Kon et al., 2021; Wu et al., 2014), particularly systemic infections caused by *Pseudomonas plecoglossicida*, which result in severe tissue necrosis, systemic damage, and high mortality rates. Such infections trigger robust inflammatory responses, characterized by elevated pro-inflammatory cytokine expression (Tang et al., 2020; Yuan et al., 2022). This pathogen exhibits sophisticated immune evasion strategies, including inhibition of phagocytosis and manipulation of immune signaling pathways (Sun et al., 2019; Tao et al., 2020; Wu et al., 2022), making it an ideal candidate for studying inflammasome-mediated immune mechanisms. Additionally, the zebrafish (*Danio rerio*, *Dr*) was used as a representative PYD-containing Caspase-1 inflammasome model for comparative study. Together, these two teleost species facilitated a systematic investigation into the palmitoylation-mediated activation of the NLRP3 inflammasome in teleosts. Our findings revealed a previously unrecognized palmitoylation-dependent mechanism for NLRP3 activation, with palmitoylation sites and palmitoyl transferase pathways distinct from that described in mammals. Specifically, a teleost-specific cysteine residue (C946 in *Lc*NLRP3, C1037 in *Dr*NLRP3) was identified as the site of palmitoylation by zDHHC18, a modification essential for NLRP3 translocation to the dispersed trans-Golgi network (dTGN) and subsequent localization to the microtubule-organizing center (MTOC). This membrane trafficking event is critical for inflammasome assembly and subsequent initiation of immune responses. This species-specific palmitoylation event highlights a unique regulatory adaptation in teleosts, suggesting a co-evolution of palmitoyl transferases and palmitoylation mechanisms in teleosts, enabling fine-tuned immune responses adapted to their specific environmental challenges.

MATERIALS AND METHODS

Fish and ethics statements

Large yellow croakers (100±20 g) were purchased from a maricultural farm in Xiangshan County, Ningbo, China, and were maintained at 25°C in a flow-through seawater system. Fish were acclimated to this environment for at least two weeks prior to use in experiments. All experiments involving animals were approved by the Ningbo University Institutional Animal Care and Use Committee (approval No. 12838) and were carried out in compliance with the National Institutes of Health's Guide for the Care and Use of Laboratory Animals.

Antibodies

Antibodies and compounds used in this study included: anti-TOMM20 (1:200, #sc-17764, Santa Cruz Biotechnology, USA), anti-Calnexin (1:100, #sc-23954, Santa Cruz Biotechnology, USA), anti-γ-tubulin (1:500, #T6557, Sigma Aldrich, USA), anti-TGN46 (1:100, #sc-166594, Santa Cruz Biotechnology, USA), anti-ninein (1:100, #sc-376420, Santa Cruz Biotechnology, USA), goat anti-mouse IgG2b Cross-adsorbed secondary antibody, Alexa Fluor™ 555 (1:500, #A-21147, Thermo Fisher Scientific, USA), goat anti-rabbit IgG (H+L) cross-adsorbed secondary antibody, Alexa Fluor™ 488 (1:500, #A-11008, Thermo Fisher Scientific, USA), goat anti-rabbit IgG, horseradish-peroxidase (HRP) conjugated secondary antibody (1:3000, #M21002, Abmart, China), goat anti-mouse IgG, HRP conjugated secondary antibody (1:3000, #M21001, Abmart, China), mouse anti-HA (1:3000, #M20003, Abmart, China), rabbit anti-HA (1:3000, #TT0050, Abmart, China), rabbit anti-FLAG tag (1:3000, #TT0053, Abmart, China), mouse anti-FLAG tag (1:3000, #M20008, Abmart, China), mouse anti-Myc (1:3000, #M20002, Abmart, China), anti-β-tubulin (1:2000, #M20005, Abmart, China), anti-GAPDH (1:2000, M20006, Abmart, China), anti-FLAG® M2 affinity gel (#A2220, Sigma-Aldrich, USA), monoclonal anti-HA-agarose (#A2095, Sigma-Aldrich, USA).

Plasmids

Various plasmids, including pcDNA3-*Lc*NLRP3-Flag, pcDNA3-*Lc*NLRP3-HA, pcDNA3-*Lc*Pro-Caspase-1-Flag, pcDNA3-*Lc*Pro-Caspase-1-HA, pcDNA3-*Lc*Pro-Caspase-1-Myc, pcDNA3-*Lc*ASC-HA, pcDNA3-*Lc*ASC-Myc, pcDNA3-*Lc*GSDME-HA, and pcDNA3-*Lc*GSDME-Flag, were generated in this study. The 22 pcDNA3-*Lc*ZDHHCs-HA plasmids were previously constructed by our lab (Dai et al., 2024). Primer sequences used in this study are provided in Supplementary Table S1.

Cell culture and bacteria

HEK293T cells were cultured in Dulbecco's Modified Eagle Medium (DMEM, #11966025, Gibco, Thermo Fisher Scientific, USA) supplemented with 10% (v/v) fetal bovine serum (FBS, #26140079, Thermo Fisher Scientific, USA) and 1% penicillin/streptomycin (#15140148, Thermo Fisher Scientific, USA). The HEK293T cells were originally obtained from the Cell Bank of the Shanghai Institute of Biochemistry and Cell Biology (https://www.cellbank.org.cn/) and cultured at 37°C with 5% CO_2.

Large yellow croaker primary head kidney monocytes/macrophages (*Lc*MO/MΦs) were isolated and cultured as described in previous research, with minor modifications (Li et al., 2020a). Briefly, fish were immersed in near-freezing water for 30 min to mitigate pain or stress and after a lethal blow to the head, head kidneys were aseptically removed and homogenized using a sterile syringe plunger through a 100 μm nylon cell strainer (#352360, Corning, USA) in RPMI1640 medium (#11875093, Thermo Fisher Scientific, USA). Cell suspensions (1 mL) were layered on 4 mL of Ficoll (45-001-751, Thermo Fisher Scientific, USA), followed by centrifugation at 400 ×*g* for 30 min at room temperature. The buffy coat layer was then collected, and cells were twice washed in RPMI1640 medium. Isolated cells were seeded in 6-well plates and grown at 24°C and 5% CO_2 in complete RPMI1640 medium supplemented with 5% fish serum, 5% FBS, and 1% penicillin/streptomycin. After overnight incubation, non-adherent cells were removed prior to experiments.

Gram-negative *P. plecoglossicida* strains were a kind gift from Professor Yan's Lab (Huang et al., 2018). Briefly, the bacteria were grown at 18°C with shaking in nutrient broth medium (#12795084, Thermo Fisher Scientific, USA). Cells were harvested at the logarithmic growth phase by centrifugation at 5 000 ×*g* for 15 min at room temperature and washed with sterile phosphate-buffered saline (PBS) prior to usage.

Antibody preparation

Rabbit polyclonal antibodies against *Lc*pro-Caspase-1 p10 (anti-*Lc*pro-Caspase-1) were generated. Briefly, a 15 amino acid sequence "CEGLPFRNIRQMPTK" within the p10 subunit of *Lc*pro-Caspase-1 was synthesized and conjugated to keyhole limpet hemocyanin (KLH) proteins, with further immunization, serum collection, antibody purification, and validation performed by the GenScript Biotech Corporation (China).

***Lc*NLRP3 inflammasome activation and immunoblotting**

To examine endogenous *Lc*NLRP3 inflammasome activation, *Lc*MO/MΦs (1×10^6 cells) were primed with lipopolysaccharide (LPS; #L7895, Sigma Aldrich, USA) at a concentration of 10 μg/mL for 8 h, followed by nigericin (#N7143, Sigma Aldrich, USA; 40 μmol/L) or adenosine triphosphate (ATP, A7699, Sigma Aldrich, USA; 5 mmol/L) activation for 1 h and 5 h, respectively. Alternatively, *Lc*MO/MΦs (1×10^6 cells) were infected with *P. plecoglossicida* at a multiplicity of infection (MOI) of 10 for the indicated time points.

To examine exogenous *Lc*NLRP3 inflammasome activation, key components and downstream effectors, including *Lc*NLRP3, *Lc*ASC, *Lc*pro-Caspase-1, and/or *Lc*GSDME were cloned into respective constructs, which were cotransfected (1 μg/10^6 cells) into HEK293T cells using Lipofectamine 3000 (#L3000015, Thermo Fisher Scientific, USA) for 24 h. The transfected cells were subsequently trypsinized, reseeded, subjected to various stimulation groups for further analysis.

To investigate the impact of palmitoylation on *Lc*NLRP3 inflammasome activation, cells were treated with palmitoylation activators and inhibitors, including palmitic acid (#P5585, Sigma Aldrich, USA; 200 μmol/L), 2-bromohexadecanoic acid (2-BP; #21604, Sigma Aldrich, USA; 100 μmol/L), and palmostatin B (Palm B; #508738, Sigma Aldrich, USA; 5 μmol/L). These treatments were applied during the priming stage for 12 hours and maintained throughout the assays.

Immunoblotting was further performed to detect cleavage products of *Lc*pro-Caspase-1 and *Lc*GSDME. Briefly, cells were lysed in pre-chilled RIPA lysis buffer (#89901, Thermo Fisher Scientific, USA) supplemented with a protease inhibitor cocktail (#A32965, Thermo Fisher Scientific, USA). After 30 min of lysis on ice, lysates were mixed with 4×Laemmli buffer (#1610747, Bio-Rad, USA) and denatured at 100°C for 12 min, followed by centrifugation for 30 s at 13 000 ×*g* at room temperature. Denatured samples were then resolved using sodium dodecyl-sulfate polyacrylamide gel electrophoresis (SDS-PAGE) and transferred to nitrocellulose membranes (#GE10600007, Sigma Aldrich, USA). The membranes were then incubated for 1 h in 5% skim milk and probed using respective primary antibodies at 4°C. After overnight incubation, membranes were incubated at room temperature in respective HRP-conjugated secondary antibodies for 1 h. Immunoreactive bands were detected using an ECL western blotting substrate (#32106, Thermo Fisher Scientific, USA; #WBKLS0500, Millipore, USA), followed by exposure to X-ray films.

Cellular transfection and co-immunoprecipitation

HEK293T cells were used to reconstitute the LcNLRP3 inflammasome due to their high transfection efficiency and lack of endogenous NLRP3 inflammasome components, making them an ideal "bioreactor" for studying inflammasome components and interactions from other species, as demonstrated in many studies (He et al., 2016b; Li et al., 2020b; Shi et al., 2016). HEK293T cells (1×10^6 cells) were cotransfected with the following plasmid combinations: Flag-*Lc*NLRP3 (2 μg) and HA-*Lc*NLRP3 (2 μg); Flag-*Lc*NLRP3 (2 μg) and HA-*Lc*ASC (2 μg); HA-*Lc*pro-Caspase-1 (2 μg) and Myc-*Lc*ASC (3 μg); Flag-*Lc*NLRP3 (2 μg), Myc-*Lc*ASC (3 μg), and HA-*Lc*pro-Caspase-1 (2 μg); HA-*Lc*NLRP3 (2 μg) and Flag-*Lc*NLRP3-C946A (2 μg; cysteine 946 mutated to alanine); and HA-*Lc*ASC (2 μg) and Flag-*Lc*NLRP3-C946A (2 μg). Briefly, the specified amounts of plasmids were transfected into HEK293T cells using Lipofectamine 3000 (#L3000015, Thermo Fisher Scientific, USA). After 48 h, the cells were lysed in pre-chilled RIPA lysis buffer supplemented with a protease inhibitor cocktail. The lysates were incubated

on ice for 30 min, then centrifuged at 13 000 ×*g* for 5 min at 4°C. The resulting supernatants were incubated overnight at 4°C under gentle rotation with anti-FLAG M2 affinity gel (#A2220, Sigma Aldrich, USA) or anti-HA (#2095, Sigma Aldrich, USA) agarose beads. The agarose beads were subsequently washed five times with wash buffer (10 mmol/L Tris-HCl (pH 7.5), 10 mmol/L KCl, 1.5 mmol/L $MgCl_2$, 500 mmol/L NaCl, 0.1% Tween 20) prior to SDS-PAGE and western blot analyses as detailed above using respective antibodies.

To identify potential palmitoyl transferases interacting with *Lc*NLRP3, HEK293T cells were cotransfected with Flag-*Lc*NLRP3 (2 μg) and HA-zDHHC plasmids (2 μg) using Lipofectamine 3000. After 48 h, the cells were lysed, co-immunoprecipitated, and immunoblotted as described above.

Acyl-biotin exchange (ABE) assay

The ABE assay was performed to analyze the palmitoylation status of *Lc*NLRP3, following previously described protocols (Balasubramanian et al., 2024). In brief, HEK293T cells were transfected with the Flag-*Lc*NLRP3 (3 μg) or Flag-*Dr*NLRP3 (3 μg) constructs or their respective mutants, or cotransfected with Flag-*Lc*NLRP3 (3 μg) and HA-*Lc*ZDHHC5/9/17/18 (2 μg), using Lipofectamine 3000. After 48 h, cells were sonicated for 30 s (2 s intervals, 20 kHz) in PBS supplemented with protease inhibitor cocktail. Sonicated samples were centrifuged at 13 000 ×*g* for 5 min at 4°C and the resulting supernatants were assayed to determine total protein (#5000002, Bio-Rad, USA). Collected supernatants (3 mg of protein) were then incubated with blocking buffer (250 mmol/L HEPES pH 7.4, 1 mmol/L EDTA, 2.5% SDS, 20 mmol/L methyl methanethiosulfonate (MMTS; #208795, Sigma Aldrich, USA)) at 50°C for 40 min with constant shaking to block free thiols and were precipitated three times with chloroform/methanol/water (v/v 1:4:3) to remove the remaining MMTS. Samples were then equally divided into two parts and incubated with HAM buffer (0.7 mol/L hydroxylamine (#55460, Sigma Aldrich, USA), 1 mmol/L BiotinHPDP (#16459, Cayman Chemical, USA), 0.2% Triton X-100, 0.1% protease inhibitor cocktail) or a negative control (50 mmol/L HEPES, 1 mmol/L biotin-HPDP, 0.2% Triton X-100, 0.1% protease inhibitor cocktail) at room temperature for 1 h. The samples were precipitated again, resolved, and diluted with dilution buffer (20 mmol/L HEPES pH 7.4, 100 mmol/L NaCl, 1 mmol/L EDTA, 0.5% Triton X-100, 0.1% protease inhibitor cocktail) to reach an SDS concentration compatible with avidin capture, then incubated with 30 μL of streptavidin beads (#20347, Thermo Fisher Scientific, USA) with shaking at 4°C for 1 h. The beads were washed three times with wash buffer (20 mmol/L HEPES pH 7.4, 600 mmol/L NaCl, 1 mmol/L EDTA, 0.5% Triton X-100, 0.1% protease inhibitor cocktail), followed by a final wash with dilution buffer. The beads were then mixed with 2×Laemmli buffer (#1610737EDU, Bio-Rad, USA) and denatured at 95°C for 10 min prior to SDS-PAGE and western blot analyses using indicated antibodies, as detailed above.

Immunofluorescence and live cell microscopy

For immunofluorescence microscopy, HEK293T cells were transfected or cotransfected with following plasmid combinations: Flag-*Lc*NLRP3 (1 μg); Flag-*Lc*ASC (1 μg); Flag-*Lc*NLRP3-C946A (1 μg); HA-*Lc*zDHHC18 (1 μg); Flag-*Lc*NLRP3 (1 μg) and HA-*Lc*NLRP3 (1 μg); Myc-*Lc*ASC (1.5 μg) and Flag-*Lc*pro-Caspase-1 (1 μg); HA-*Lc*ASC(1 μg) and Flag-*Lc*NLRP3-C946A (1 μg); and Flag-*Lc*NLRP3 (1 μg) and HA-*Lc*zDHHC18 (1 μg) for 24 h, then seeded at a density of 2×10^5 cells/mL on coverslips. In some experiments, cells were pre-treated with PA (200 μmol/L) or 2-BP (100 μmol/L) during transfection. After 24 h of cultivation on coverslips, the cells were stimulated with nigericin (40 μmol/L) for 1 h or directly fixed with 4% paraformaldehyde in sterile PBS at room temperature for 15 min. The cells were then permeabilized with 0.25% Triton X-100 (for GTU and Ninein) or 0.5% saponin (for TGN46, TOMM20, Calnexin and Flag-, HA- and Myc-tagged proteins) for an additional 15 min before incubation in PBS containing 5% BSA for 1 h at room temperature. After blocking, the cells were labeled with respective primary and secondary antibodies, with the nuclei then visualized by 4',6-diamidino-2-phenylindole (DAPI) staining (#62248, Thermo Fisher Scientific, USA).

For live cell imaging, HEK293T and *Lc*MO/MΦ cell models were used to observe pyroptosis. Briefly, HEK293T cells (1×10^6) were transfected or cotransfected with the following plasmid combinations: HA-*Lc*GSDME (2 μg); HA-*Lc*GSDME (2 μg) and Flag-*Lc*NLRP3 (2 μg); HA-*Lc*GSDME (2 μg) and Flag-*Lc*pro-Caspase-1 (2 μg); HA-*Lc*GSDME (2 μg) and HA-*Lc*ASC (2 μg); and HA-*Lc*GSDME (2 μg), Flag-*Lc*NLRP3 (2 μg)/Flag-*Lc*NLRP3-C946A (2 μg), Flag-*Lc*pro-Caspase-1 (2 μg), and HA-*Lc*ASC (2 μg). After 48 h of transfection, the cells were incubated in culturing medium containing 20 nmol/L SYTOX Green (#S7020, Thermo Fisher Scientific, USA) for 4 h before nigericin (40 μmol/L) stimulation for an additional 1 h at 37°C. *Lc*MO/MΦ cells (1×10^6) were cultured in medium containing 20 nmol/L SYTOX Green for 4 h, then stimulated with *P. plecoglossicida* (MOI=10) or primed with LPS (10 μg/mL) for 8 h followed by ATP (5 mmol/L) or nigericin (40 μmol/L) activation for indicated time points at 26°C. All culture dishes for live cell imaging were placed into a microscope stage chamber supplemented with 5% CO_2 and heated to 37°C or 26°C.

All images were collected and analyzed using a Zeiss LSM 880 confocal microscope (Carl Zeiss AG, Germany) and ZEN Blue software (Carl Zeiss AG, Germany), respectively.

Lactate dehydrogenase (LDH) assay

LDH release was measured in cell culture supernatants immediately after the experiments using the CytoTox96® Non-Radioactive Cytotoxicity Assay (#G1780, Promega, USA), following the manufacturer's instructions. Results were normalized to a lysis control, with background values from blank medium subtracted.

siRNA interference

To knockdown *zDHHC18* expression in *Lc*MO/MΦs, *Lc*MO/MΦ cells were transfected with 1 μg of *zDHHC18* siRNAs using Lipofectamine™ RNAiMAX (#13778150, Thermo Fisher Scientific, USA), according to the manufacturers' instructions. After 48 h of transfection, the cells were collected, followed by total RNA isolation and reverse transcription-quantitative real-time polymerase chain reaction (RT-qPCR). The siRNA sequences used included: Scramble control, 5'-ACGGTGTACTGCGGATCTAACCA-3'; *LcZDHHC18* siRNA #1, 5'-GTTTCTTCTACACCTTCAT-3'; *LcZDHHC18* siRNA #2, 5'-CCAGAGCTTTCAACAAGCT-3'; and *LcZDHHC18* siRNA #3, 5'-CGTGATATGTTTCTTCTCA-3'.

Model building and structure representation

The tertiary structures of *Lc*ZDHHC18 and *Dr*ZDHHC18 were

analyzed and modeled using SWISS-MODEL (https://swissmodel.expasy.org/interactive). To explore the structural characteristics of oligomerized *Lc*NLRP3, the six-fold double-ring cage structure of mouse NLRP3 (PDB ID: 7LFH) was used as a template in SWISS-MODEL. The *Lc*NLRP3 protein sequence was applied to generate homology models of oligomerized *Lc*NLRP3.

Quantification and statistical analysis

Data are presented as mean±standard deviation (SD). Statistical analyses were performed using GraphPad Prism v.8. Differences among multiple groups were analyzed using one-way analysis of variance (ANOVA), followed by Tukey's multiple comparison tests, while differences between two groups were assessed using Student's *t*-tests. Statistical significance was denoted as *: $P<0.05$ and **: $P<0.01$.

RESULTS

NLRP3 palmitoylation is required for inflammasome activation in teleosts

To investigate the regulatory mechanisms of NLRP3 inflammasome activation in teleosts, we characterized the assembly and function of the large yellow croaker NLRP3 (*Lc*NLRP3) inflammasome, building upon prior studies of the zebrafish NLRP3 (*Dr*NLRP3) (Li et al., 2020b). Structural analyses suggested that, similar to its mammalian counterpart, *Lc*NLRP3 oligomerized to a cage-like configuration (Andreeva et al., 2021) (Supplementary Figure S1A, B) and interacted with the adaptor molecule *Lc*ASC (Supplementary Figure S1C), which subsequently recruited *Lc*pro-Caspase-1 to assemble the *Lc*NLRP3 inflammasome (Supplementary Figure S1D). Notably, the presence of *Lc*ASC was required for the interaction between *Lc*NLRP3 and *Lc*pro-Caspase-1 (Supplementary Figure S1E, F). Additionally, the presence of all three components and stimulation with nigericin (a common NLRP3 activator) were required for the *Lc*NLRP3 inflammasome to induce *Lc*pro-caspase-1 cleavage, resulting in the formation of the p10 band (Figure 1A; Supplementary Figure S1G). Correspondingly, cleavage of the downstream effector *Lc*GSDME was observed, along with induction of pyroptosis and release of lactate dehydrogenase (LDH). These effects were only observed in cells co-expressing *Lc*NLRP3, *Lc*ASC, and *Lc*pro-Caspase-1 and subjected to nigericin stimulation (Figure 1B, C; Supplementary Figure S1H). *In vivo* analyses further confirmed that stimulation with classical NLRP3 activators (LPS priming followed by nigericin or ATP) or infection with *P. plecoglossicida* induced robust *Lc*NLRP3 inflammasome formation and subsequent *Lc*pro-Caspase-1 cleavage, generating the p10 fragment (Figure 1D; Supplementary Figure 1I) and ultimately leading to pyroptosis in head kidney-derived *Lc*MO/MΦs (Supplementary Figure S1J).

The dynamic membrane trafficking of mammalian NLRP3, involving the TGN, mitochondria, and endoplasmic reticulum (ER), has been extensively documented in the context of inflammasome activation (Arumugam et al., 2022; Chen & Chen, 2018; Zhou et al., 2020). However, the role of membrane translocation in teleost NLRP3 inflammasome activation and the precise site of inflammasome assembly remain unexplored. Our results showed that, under resting conditions, *Lc*NLRP3 exhibited a diffuse cytoplasm distribution without specific localization to the dTGN, mitochondria, or ER membranes (Supplementary Figure S1K). Upon nigericin stimulation, *Lc*NLRP3 translocated primarily to the dTGN membrane, with no significant association with mitochondria or ER membranes (Figure 1E). Additionally, *Lc*NLRP3 inflammasome assembly occurred at the MTOC, as evidenced by the formation of *Lc*NLRP3-ASC specks and the colocalization of *Lc*NLRP3, *Lc*ASC, and *Lc*Caspase-1 with the MTOC marker GTU (Figure 1F, G). These observations indicate that teleost NLRP3 inflammasome activation also requires TGN-mediated translocation of *Lc*NLRP3 to the MTOC, where inflammasome assembly occurs.

Palmitoylation, a lipid modification known to mediate protein membrane targeting (Bijlmakers & Marsh, 2003; Rocks et al., 2010), was investigated as a potential regulator of teleost NLRP3 activation, based on prior evidence suggesting the involvement of zebrafish *Dr*NLRP3 in palmitoylation-mediated activation (Nie et al., 2024). In the present study, ABE assays confirmed that *Lc*NLRP3 also undergoes palmitoylation (Drisdel et al., 2006) (Supplementary Figure S2A). Notably, *Lc*NLRP3 palmitoylation levels were significantly increased following palmitate acid (PA) treatment and almost abolished in the presence of 2-BP, a palmitoyl transferase inhibitor (Figure 2A, B).

To assess the functional relevance of *Lc*NLRP3 palmitoylation, its impact on inflammasome assembly and activation was evaluated. Results showed that palmitoylation inhibition with 2-BP suppressed *Lc*NLRP3 oligomerization and reduced interactions with *Lc*ASC during inflammasome assembly (Figure 2C, D). Colocalization of *Lc*NLRP3 with the MTOC marker ninein and the formation of *Lc*NLRP3-ASC specks were substantially impaired in the presence of 2-BP, while PA treatment significantly enhanced these interactions (Figure 2E, F). These observations were consistent with functional assays: PA treatment significantly increased pyroptosis levels and LDH release, whereas 2-BP treatment led to a marked decrease in these pyroptotic responses (Figure 2G; Supplementary Figure S2B, C). Cleavage of *Lc*pro-Caspase-1 was enhanced by PA or Palm B, an acyl-protein thioesterase inhibitor, while 2-BP treatment resulted in dose-dependent inhibition (Figure 2H, I). Similar effects were observed for *Lc*GSDME cleavage and corresponding changes in LDH secretion (Figure 2J, K). Furthermore, the induced expression levels of inflammasome-related genes, including *LcNLRP3*, *LcASC*, and *LcCaspase-1*, were unaffected by 2-BP treatment (Supplementary Figure S2D), indicating that the observed decrease in downstream effector cleavage with palmitoylation inhibition was attributable to impaired inflammasome assembly rather than altered mRNA levels.

Teleost NLRP3s are palmitoylated at unique residues distinct from mammalian counterparts

Recent studies have identified several palmitoylation sites in mammalian NLRP3, each playing distinct regulatory roles in its activation and function (Hu et al., 2024; Nie et al, 2024; Wang et al, 2023; Yu et al, 2024; Zheng et al, 2023). However, key residues implicated in palmitoylation, such as C130 and C958 in human and mouse NLRP3, are absent in teleost NLRP3 (Supplementary Figure S2E), indicating potential evolutionary divergence. Therefore, teleost NLRP3 was screened for possible palmitoylation sites based on predictions by GPS-Palm (http://gpspalm.biocuckoo.cn/download.php). A unique cysteine residue (C946 in *Lc*NLRP3 and C1037 in *Dr*NLRP3) was identified, which exhibited the

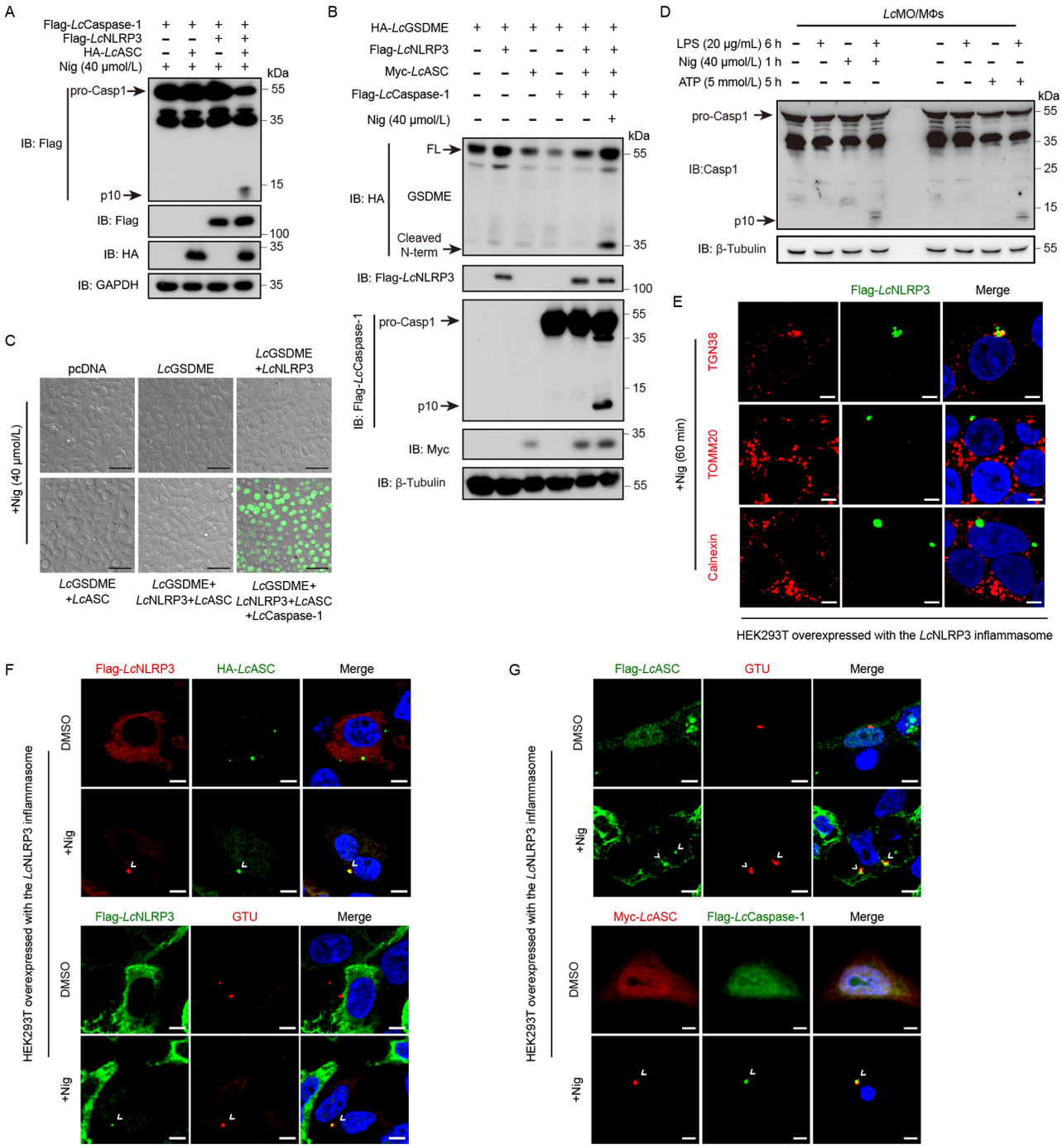

Figure 1 Components and activation of large yellow croaker NLRP3 inflammasome

A: Caspase-1 processing (p10) in nigericin (40 μmol/L)-stimulated HEK293T cells overexpressing Flag-*Lc*Caspase-1, with or without other inflammasome components, Flag-*Lc*NLRP3, and/or HA-*Lc*ASC. B: Gasdermin E (cleaved N-term) processing in HEK293T cells overexpressing HA-*Lc*GSDME, with or without Flag-*Lc*NLRP3, Myc-*Lc*ASC, and/or Flag-*Lc*Caspase-1, stimulated with nigericin (40 μmol/L) or not. C: Live cell imaging of pyroptosis in nigericin (40 μmol/L)-stimulated HEK293T cells overexpressing HA-*Lc*GSDME, with or without other inflammasome components, using SYTOX Green for nucleic acid staining. Scale bars: 50 μm. D: Caspase-1 processing (p10) upon NLRP3 inflammasome activation in isolated large yellow croaker head kidney *Lc*MO/MΦs primed with LPS and stimulated with nigericin or ATP for 60 min. E: Immunofluorescence images showing colocalization of *Lc*NLRP3 with TGN38 (trans-Golgi network marker), TOMM20 (mitochondria marker), and calnexin (ER marker) in HEK293T cells overexpressing *Lc*NLRP3 inflammasome components and stimulated with nigericin. Scale bars: 5 μm. F: Immunofluorescence images showing formation of *Lc*NLRP3-ASC puncta and colocalization of NLRP3 puncta with MTOC marker GTU in HEK293T cells overexpressing *Lc*NLRP3 inflammasome components, with or without nigericin stimulation. Scale bars: 5 μm. G: Immunofluorescence images showing colocalization of ASC puncta with MTOC marker GTU and colocalization of *Lc*ASC and *Lc*Caspase-1 in HEK293T cells overexpressing *Lc*NLRP3 inflammasome components, with or without nigericin stimulation. Scale bars: 5 μm. All immunofluorescence images are representative of three independent experiments. Blue indicates nuclear staining by DAPI. Arrowheads indicate puncta.

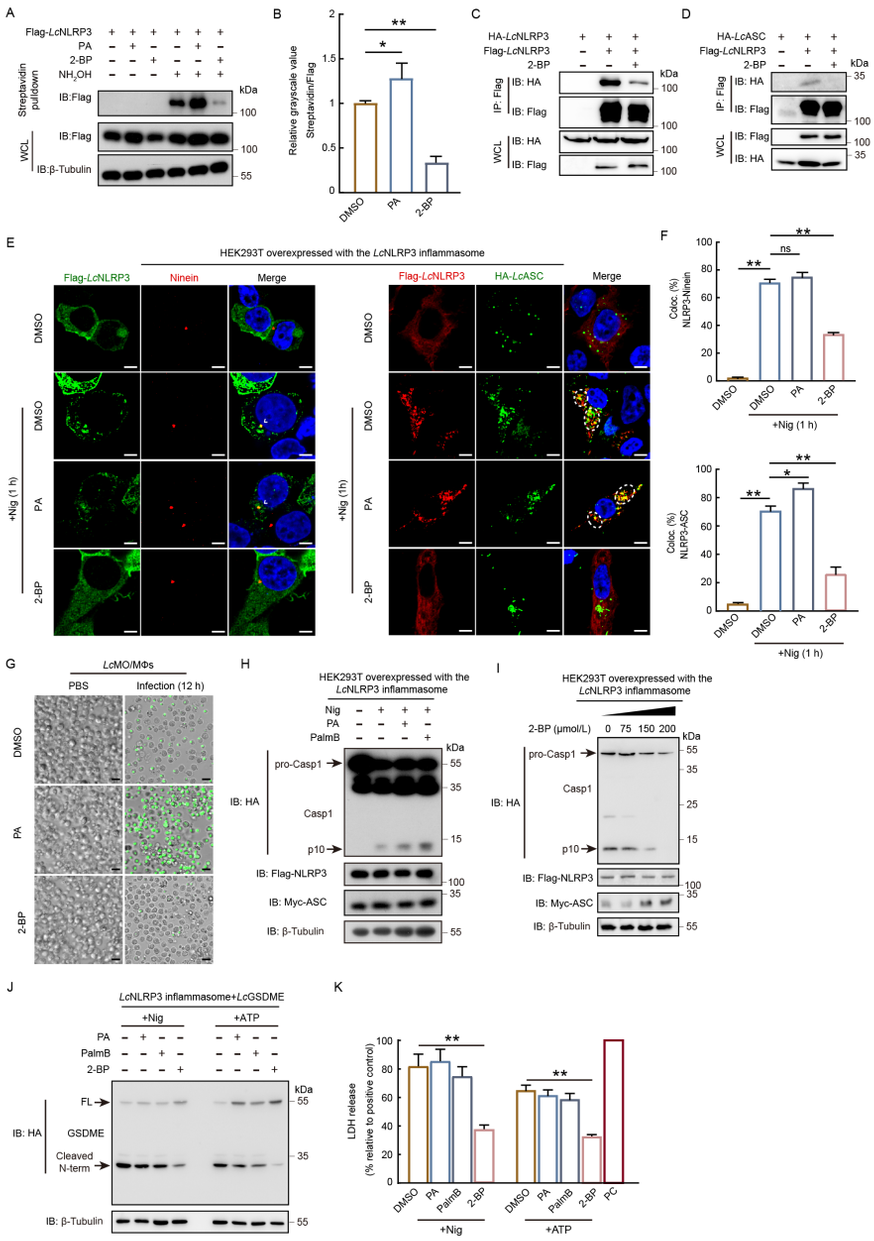

Figure 2 Palmitoylation of teleost NLRP3 is required for inflammasome activation

A: ABE assay of palmitoylation levels of Flag-*Lc*NLRP3 expressed in HEK293T cells treated with PA (200 μmol/L) or 2-BP (100 μmol/L), with or without hydroxylamine. B: Semi-quantitative analysis of relative grayscale values of immunoblot bands from (A) to evaluate S-palmitoylation levels of *Lc*NLRP3 in each group. Mean±SD, *n*=3. *: *P*<0.05; **: *P*<0.01. Data were analyzed using an unpaired two-tailed Student's *t*-test. C: Immunoblotting of whole-cell lysate (WCL) and anti-Flag IPs derived from HEK293T cells transfected with HA-*Lc*NLRP3 and Flag-*Lc*NLRP3, with or without 2-BP (100 μmol/L), to examine *Lc*NLRP3 oligomerization. D: Immunoblotting of WCL and anti-Flag IPs derived from HEK293T cells transfected with HA-*Lc*ASC and Flag-*Lc*NLRP3, with or without 2-BP (100 μmol/L), to examine interactions between *Lc*NLRP3 and *Lc*ASC. E: Immunofluorescence images showing colocalization of *Lc*NLRP3 puncta with MTOC marker ninein or formation of *Lc*NLRP3-ASC puncta in HEK293T cells overexpressing *Lc*NLRP3 inflammasome components, with or without nigericin stimulation, in the presence of PA (200 μmol/L) or 2-BP (100 μmol/L). Blue indicates nuclear staining by DAPI. Arrowheads indicate puncta; dashed circles indicate colocalization areas. Scale bars: 5 μm. F: Quantification of percentage of cells exhibiting *Lc*NLRP3-ninein or *Lc*NLRP3-ASC colocalization in (E). Mean±SD, *n*=3 fields, *: *P*<0.05; **: *P*<0.01; ns: Not significant. Data were analyzed using an unpaired two-tailed Student's *t*-test. G: Live cell imaging of pyroptosis in *Lc*MO/MΦs infected with *P. plecoglossicida* for 12 h, using SYTOX Green nucleic acid staining, in the presence of PA (200 μmol/L) or 2-BP (100 μmol/L). Scale bars: 50 μm. H: Caspase-1 processing (p10) in HEK293T cells overexpressing *Lc*NLRP3 inflammasome components, with or without nigericin (40 μmol/L) stimulation, in the presence of PA (200 μmol/L) or Palm-B (5 μmol/L). I: Caspase-1 processing (p10) in nigericin (40 μmol/L)-stimulated HEK293T cells overexpressing *Lc*NLRP3 inflammasome components, treated with increasing concentrations of 2-BP. J: Gasdermin E (cleaved N-term) processing in nigericin or ATP-stimulated HEK293T cells overexpressing *Lc*NLRP3 inflammasome components and *Lc*GSDME, in the presence of PA (200 μmol/L), Palm-B (5 μmol/L), or 2-BP (100 μmol/L). K: Relative LDH release levels in nigericin or ATP-stimulated HEK293T cells overexpressing *Lc*NLRP3 inflammasome components and *Lc*GSDME. Mean±SD, *n*=3, **: *P*<0.01. Data were analyzed using an unpaired two-tailed Student's *t*-test.

highest probability of palmitoylation (Supplementary Figure S2E), suggesting an adaptive modification distinct from mammalian counterparts.

Palmitoylation at this site was further investigated, alongside corresponding palmitoylation sites identified in mammalian NLRP3 (C837/844 in human NLRP3, corresponding to C778/785 in *Lc*NLRP3 and C867/874 in *Dr*NLRP3). Mutation of C946 or C1037 to alanine (C946A/C1037A) significantly reduced palmitoylation levels, while mutations at C778/785 or C867/874 had no detectable effect (Figure 3A–D). Structural modeling indicated that C946 residue was located in the LRR domain of *Lc*NLRP3, with a palmitic acid chain at this site likely enhancing the "face to face" interactions between monomers during oligomerization, predominantly associated with membranes (Andreeva et al., 2021) (Supplementary Figures S1B, S2F). Consistently, the interaction between *Lc*NLRP3 monomers was substantially weakened in the C946A mutant compared to the wild-type (WT) *Lc*NLRP3 (Figure 3E). Moreover, mutation of C946 inhibited the interaction between *Lc*NLRP3 and *Lc*ASC, indicating failed inflammasome assembly (Figure 3F).

To further assess the physiological significance of this teleost-specific palmitoylation site, the role of C946 was assessed in NLRP3 inflammasome activation using the large yellow croaker homolog as a model. Overexpression of either WT *Lc*NLRP3 or the C946A mutant, along with *Lc*ASC, in HEK293T cells revealed that C946 mutation substantially decreased the colocalization of *Lc*NLRP3 with the MTOC marker ninein and disrupted the formation of NLRP3-ASC puncta at the MTOC (Figure 3G). In line with these findings, cleavage of *Lc*pro-Caspase-1 and *Lc*GSDME, as well as pyroptosis and LDH secretion, were significantly diminished in cells reconstituted with the C946A mutant (Figure 3H–K).

Palmitoylation regulates teleost NLRP3 membrane translocation

Palmitoylation, a crucial post-translational protein modification, facilitates protein targeting to subcellular membranes (Rocks et al., 2010). Our results demonstrated that teleost NLRP3, similar to its mammalian counterparts, localized to the dTGN membrane during activation and subsequently translocated to the MTOC for inflammasome assembly and downstream inflammatory events. Notably, none of the known palmitoylation sites in mammalian NLRP3 were conserved or palmitoylated in teleost NLRP3 (Figure 3B, D; Supplementary Figure S2E). Therefore, we further investigated whether the identified teleost-specific palmitoylation site regulates NLRP3 trafficking to the dTGN and its subsequent translocation to the MTOC.

Detailed analysis of *Lc*NLRP3 membrane trafficking during inflammasome activation (Figures 1E–G, 2E) and the conservation of this palmitoylation event across teleost species (Supplementary Figure S2E) highlighted the significance of the C946 residue in *Lc*NLRP3. Inhibition of palmitoylation by 2-BP significantly impaired dTGN localization of *Lc*NLRP3 (Figure 3L). Consistently, mutation of the palmitoylated C946 residue prevented *Lc*NLRP3 translocation to the dTGN membrane, with no detectable localization on mitochondria or ER membranes (Figure 3M). Collectively, these findings suggest that palmitoylation at this unique teleost residue is critical for the proper localization of teleost NLRP3 on dTGN vesicles, thus enabling dTGN-mediated transportation of teleost NLRP3 to the MTOC, where inflammasome assembly occurs.

zDHHC18 serves as the primary palmitoyl transferase mediating teleost NLRP3 palmitoylation

Palmitoylation is mediated by a family of palmitoyl transferases, known as aspartate-histidine-histidine-cysteine (DHHC) enzymes (Lemonidis et al., 2015). Based on 22 recently identified zDHHCs in large yellow croaker (Dai et al., 2024), immunoprecipitation experiments in HEK293T cells were conducted on teleost NLRP3-interacting proteins, using *Lc*NLRP3 as a model. Results revealed interactions between *Lc*NLRP3 and four zDHHC enzymes, including *Lc*zDHHC5, *Lc*zDHHC9, *Lc*zDHHC17 and *Lc*zDHHC18 (Supplementary Figure S3A). However, only ectopic overexpression of *Lc*zDHHC18 significantly increased *Lc*NLRP3 palmitoylation levels, establishing it as the primary palmitoyl transferase for this modification (Figure 4A).

The interaction between *Lc*zDHHC18 and *Dr*NLRP3 was further validated, given the high conservation of zDHHC18 across teleost species (Supplementary Figure S3B). Results demonstrated that *Dr*NLRP3 indeed interacted with *Lc*zDHHC18, and overexpression of *Lc*zDHHC18 increased *Dr*NLRP3 palmitoylation levels (Supplementary Figure S3C; Figure 4B). Confocal microscopy confirmed colocalization of *Lc*zDHHC18 and *Lc*NLRP3 upon nigericin stimulation (Figure 4C). These results indicate that zDHHC18 is the primary palmitoyl transferase mediating NLRP3 palmitoylation in teleosts, in contrast to the diverse zDHHC enzymes reported for mammalian NLRP3 palmitoylation.

To determine the physiological relevance of zDHHC18 in regulating teleost NLRP3 inflammasome activation, its role in *Lc*pro-Caspase-1 cleavage during *Lc*NLRP3 inflammasome activation was assessed. Overexpression of *Lc*zDHHC18, but not *Lc*ZDHHC5, *Lc*ZDHHC9, or *Lc*ZDHHC17, significantly promoted *Lc*pro-Caspase-1 cleavage in an exogenous reconstitution model (Figure 4D). To further examine its endogenous role, *Lc*zDHHC18 expression was silenced in *Lc*MO/MΦs (Supplementary Figure S3D), followed by activation of the *Lc*NLRP3 inflammasome using LPS+nigericin/ATP stimulation or *P. plecoglossicida* infection. Knockdown of *Lc*zDHHC18 significantly inhibited *Lc*pro-Caspase-1 cleavage in both activation models, mirroring the results observed in the reconstituted system (Figure 4E, F). Consistent with these observations, cell pyroptosis and LDH secretion were significantly reduced upon *Lc*zDHHC18 knockdown (Figures 4G–J). Collectively, these results establish zDHHC18 as the primary physiological palmitoyl transferase responsible for mediating teleost NLRP3 palmitoylation and its downstream functional activity, including inflammasome assembly and activation.

DISCUSSION

This study elucidated a novel mechanism of palmitoylation-mediated activation of the NLRP3 inflammasome in teleosts, using large yellow croaker and zebrafish as representative models. The components and membrane trafficking events of the teleost NLRP3 inflammasome were systematically characterized, highlighting the critical role of species-adapted palmitoylation in governing teleost NLRP3 inflammasome activation.

Recent mammalian studies have demonstrated the importance of palmitoylation in regulating NLRP3 inflammasome activation, either by promoting or inhibiting its

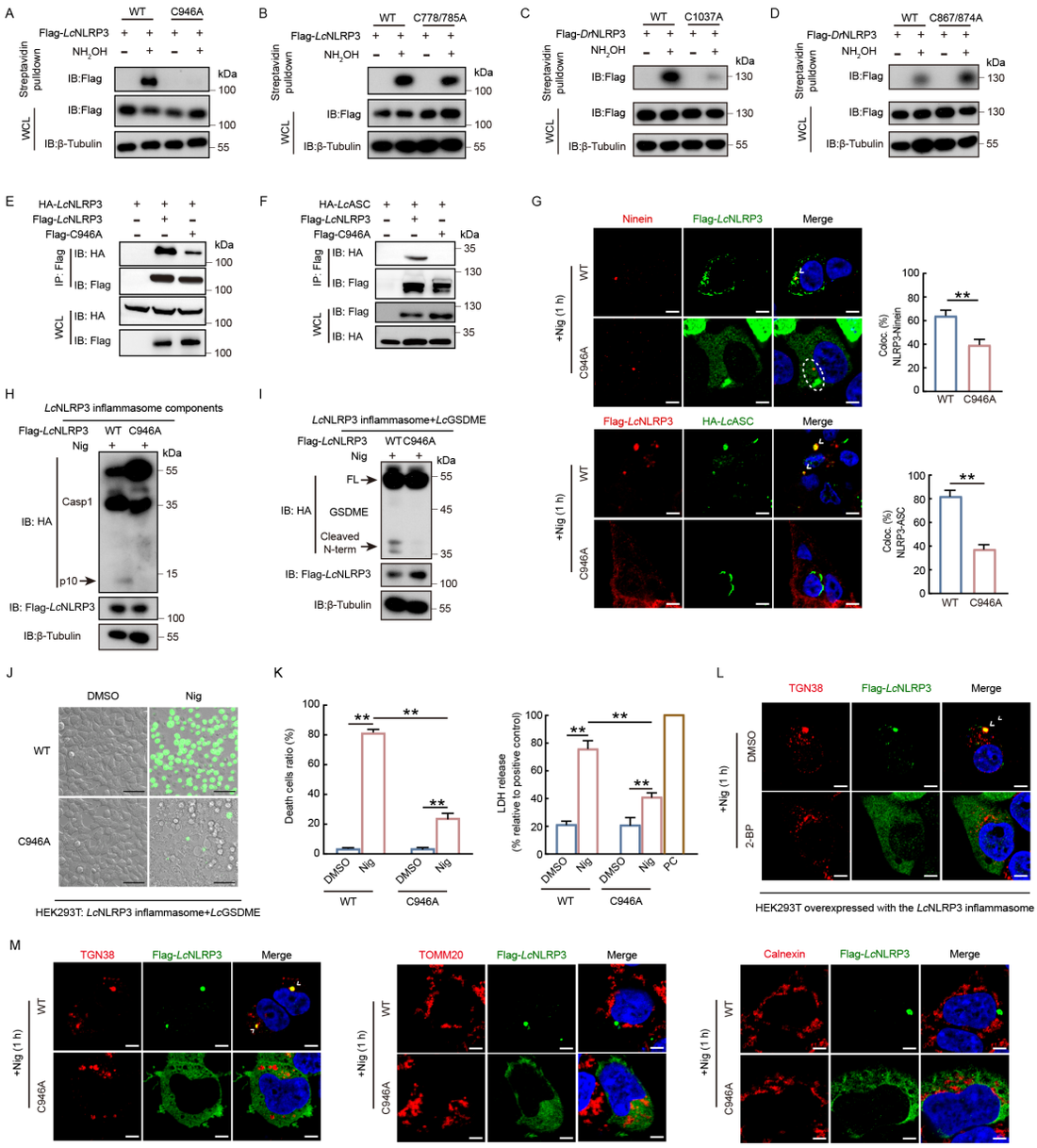

Figure 3 Palmitoylation of teleost NLRP3 at a unique residue facilitates membrane translocation

A, B: ABE assay of palmitoylation levels of Flag-*Lc*NLRP3, C946A, or C778/785A mutants overexpressed in HEK293T cells, with or without hydroxylamine. C, D: ABE assay of palmitoylation levels of Flag-*Dr*NLRP3, C1037A, or C867/874A mutants overexpressed in HEK293T cells, with or without hydroxylamine. E: Immunoblotting of WCL and anti-Flag IPs derived from HEK293T cells transfected with HA-*Lc*NLRP3 and either wild-type (WT) Flag-*Lc*NLRP3 or Flag-*Lc*NLRP3 C946A mutant to examine *Lc*NLRP3 oligomerization. F: Immunoblotting of WCL and anti-Flag IPs derived from HEK293T cells transfected with HA-*Lc*ASC and either WT Flag-*Lc*NLRP3 or Flag-*Lc*NLRP3 C946A mutant to examine interactions between *Lc*NLRP3 and *Lc*ASC. G: Immunofluorescence images showing colocalization of *Lc*NLRP3 puncta with MTOC marker ninein or formation of *Lc*NLRP3-ASC puncta in HEK293T cells overexpressing WT *Lc*NLRP3 or C946A mutant, and other inflammasome components, stimulated with nigericin. Cells exhibiting *Lc*NLRP3-ninein or *Lc*NLRP3-ASC colocalization in each group were quantified. Mean±SD, n=3 fields, **: P<0.01. Data were analyzed using an unpaired two-tailed Student's t-test. H: Caspase-1 processing (p10) in HEK293T cells overexpressing WT *Lc*NLRP3 or C946A mutant, along with other inflammasome components, stimulated with nigericin for inflammasome activation. I: Gasdermin E (cleaved N-term) processing in nigericin (40 μmol/L)-stimulated HEK293T cells overexpressing WT *Lc*NLRP3 or C946A mutant with other inflammasome components. J: Live cell imaging of pyroptosis in nigericin (40 μmol/L)-stimulated HEK293T cells overexpressing WT *Lc*NLRP3 or C946A mutant, along with other inflammasome components and HA-*Lc*GSDME, using SYTOX Green nucleic acid staining. Scale bars: 50 μm. K: Quantification of percentage of cells showing positive SYTOX Green signals and relative levels of LDH release in (I). Mean±SD, n=3, **: P<0.01. Data were analyzed using an unpaired two-tailed Student's t-test. L: Immunofluorescence images showing colocalization of *Lc*NLRP3 with trans-Golgi network marker TGN38 in nigericin (40 μmol/L)-stimulated HEK293T cells overexpressing *Lc*NLRP3 inflammasome components, with or without 2-BP (100 μmol/L). Scale bars: 5 μm. M: Immunofluorescence images showing colocalization of *Lc*NLRP3 with TGN38 (trans-Golgi network marker), TOMM20 (mitochondria marker), and calnexin (ER marker) in nigericin-stimulated HEK293T cells overexpressing WT *Lc*NLRP3 or C946A mutant with other inflammasome components. Scale bars: 5 μm. All immunofluorescence images are representative of three independent experiments. Blue indicates nuclear staining by DAPI; arrowheads indicate puncta.

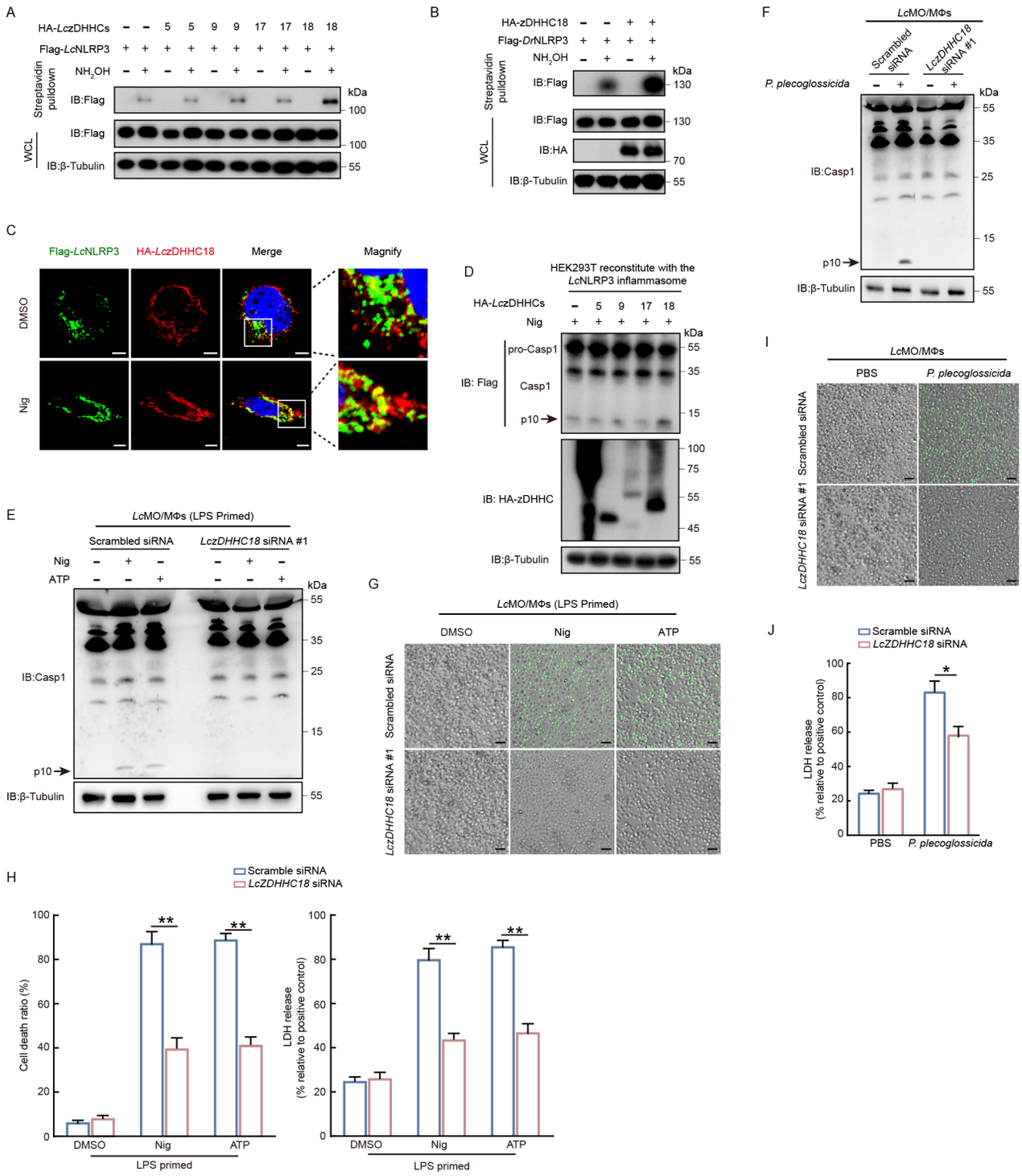

Figure 4 zDHHC18 serves as the primary palmitoyl transferase mediating teleost NLRP3 palmitoylation

A: ABE assay of palmitoylation levels of Flag-*Lc*NLRP3 in HEK293T cells overexpressing Flag-*Lc*NLRP3 alone, or with HA-*Lcz*DHHC5/9/17/18, with or without hydroxylamine. B: ABE assay of palmitoylation levels of Flag-*Dr*NLRP3 in HEK293T cells overexpressing Flag-*Dr*NLRP3 alone or with HA-*Lcz*DHHC18, with or without hydroxylamine. C: Immunofluorescence images showing colocalization of *Lc*NLRP3 and *Lcz*DHHC18 in overexpressed HEK293T cells, with or without nigericin stimulation. Blue indicates nuclear staining by DAPI. Scale bars: 5 μm. D: Caspase-1 processing (p10) in nigericin (40 μmol/L)-stimulated HEK293T cells overexpressing *Lc*NLRP3 inflammasome components, with or without HA-*Lcz*DHHC5/9/17/18. E, F: Caspase-1 processing (p10) upon NLRP3 inflammasome activation in *Lc*MO/MΦs transfected with scrambled siRNA or zDHHC18 siRNA. Cells were primed with LPS and stimulated with nigericin or ATP for 60 min (E) or infected with *P. plecoglossicida* (F) for inflammasome activation. G: Live cell imaging of pyroptosis of cells from (E) using SYTOX Green nucleic acid staining. Scale bars: 50 μm. H: Quantification of percentage of cells showing positive SYTOX Green signals and levels of LDH release in (E). Mean±SD, n=3, **: P<0.01. Data were analyzed using an unpaired two-tailed Student's t-test. I: Live cell imaging of pyroptosis of cells from (F) using SYTOX Green nucleic acid staining. Scale bars: 50 μm. J: LDH release levels in cells in (F). Mean±SD, n=3, *: P<0.05. Data were analyzed using an unpaired two-tailed Student's t-test. All immunofluorescence images are representative of three independent experiments.

function (Nie et al., 2024; Wang et al., 2023; Yu et al., 2024; Zheng et al., 2023). However, the palmitoylated residues identified in mammals are absent or not palmitoylated in teleost NLRP3 (Figure 3A–D; Supplementary Figure S2E), indicating an evolutionary adaptation specific to these species. Investigating whether palmitoylation-dependent regulatory mechanisms also exist in lower vertebrates and understanding the underlying mechanisms could offer valuable insights into the evolutionary origins and diversification of this critical innate immune platform.

C946 of *Lc*NLRP3 was identified as a conserved teleost-specific palmitoylation site through GPS-Palm predictions (Supplementary Figure S2E). Mutation of this residue to alanine abolished palmitoylation, prevented *Lc*NLRP3 localization to the dTGN and MTOC, and disrupted its interaction with *Lc*ASC at the MTOC, impairing inflammasome assembly (Figure 3A, E–M). Structural modeling suggested that palmitoylation at C946 may enhance interactions between *Lc*NLRP3 monomers, facilitating the formation of the oligomerized 'cage' structure necessary for membrane association (Supplementary Figure S2F). Similarly, the corresponding cysteine 1037 (C1037) residue in *Dr*NLRP3 also exhibited a significant reduction in palmitoylation levels when mutated, indicating that this palmitoylation event represents a teleost-specific evolutionary adaptation.

*Lc*zDHHC18 was further identified as the primary palmitoyl transferase responsible for palmitoylating *Lc*NLRP3 at C946 and *Dr*NLRP3 at C1037 (Figure 4A, B; Supplementary Figure S3A–C), differing from those mediating NLRP3 palmitoylation in mammals. Overexpression of zDHHC18 enhanced *Lc*NLRP3 and *Dr*NLRP3 palmitoylation and promoted inflammasome activation, while knockdown hindered inflammasome assembly, *Lc*pro-Caspase-1 cleavage, and cell pyroptosis (Figure 4; Supplementary Figure S3D). This teleost-specific adaptation of palmitoylation residues and transferases likely reflects evolutionary flexibility of immune regulatory mechanisms to the unique environmental challenges faced by teleosts in aquatic environments, such as fluctuating temperatures, oxygen availability, and pH levels (Blewett et al., 2022). Such challenges demand a finely tuned immune system capable of rapid and adaptive responses to diverse pathogens, such as bacteria, viruses, and parasites. Palmitoylation-mediated regulation may offer teleosts a mechanism to balance robust immune activation with the need to mitigate excessive inflammation during environmental stressors like hypoxia.

Elucidating the molecular mechanisms underpinning inflammasome activation in teleosts could lead to new strategies for managing immune-related diseases in aquaculture, where the rapid onset of immune responses is often critical for preventing large-scale outbreaks. Understanding palmitoylation-dependent regulation could inform the development of targeted vaccines or immune modulators tailored to specific teleost species, thereby improving disease resistance and overall aquaculture sustainability.

In conclusion, this study uncovered a novel palmitoylation-dependent mechanism for NLRP3 inflammasome activation in teleosts, involving a unique palmitoylation site and a distinct palmitoyl transferase. These findings advance our understanding of the molecular regulation of innate immunity and highlight the evolutionary diversity of immune mechanisms across vertebrates, thereby contributing to a cross-species understanding of the molecular basis underlying the origin and evolution of innate immunity.

SUPPLEMENTARY DATA

Supplementary data to this article can be found online.

COMPETING INTERESTS

The authors declare that they have no competing interests.

AUTHORS' CONTRIBUTIONS

Conceptualization: L.N., J.Z.S., J.C.; Methodology: L.N., C.J.F.; Investigation: L.N., X.Y.W., Z.Y.Z., C.J.F., T.F.Z.; Visualization: L.N., X.Y.W., Z.Y.Z., C.J.F., T.F.Z.; Funding acquisition: L.N., J.C.; Project administration: L.N., J.Z.S., J.C.; Supervision: L.N., J.Z.S., J.C.; Writing – original draft: L.N.; Writing – review & editing: L.N., C.J.F., J.Z.S., J.C. All authors read and approved the final version of the manuscript.

REFERENCES

Acevedo W, Morán-Figueroa R, Vargas-Chacoff L, et al. 2023. Revealing the *Salmo salar* NLRP3 inflammasome: insights from structural modeling and transcriptome analysis. *International Journal of Molecular Sciences*, **24**(19): 14556.

Andreeva L, David L, Rawson S, et al. 2021. NLRP3 cages revealed by full-length mouse NLRP3 structure control pathway activation. *Cell*, **184**(26): 6299–6312. e22.

Angosto D, López-Castejón G, López-Muñoz A, et al. 2012. Evolution of inflammasome functions in vertebrates: inflammasome and caspase-1 trigger fish macrophage cell death but are dispensable for the processing of IL-1β. *Innate Immunity*, **18**(6): 815–824.

Ao JQ, Mu YN, Xiang LX, et al. 2015. Genome sequencing of the perciform fish *Larimichthys crocea* provides insights into molecular and genetic mechanisms of stress adaptation. *PLoS Genetics*, **11**(4): e1005118.

Arumugam S, Qin YQ, Liang ZW, et al. 2022. GSK3β mediates the spatiotemporal dynamics of NLRP3 inflammasome activation. *Cell Death & Differentiation*, **29**(10): 2060–2069.

Balasubramanian A, Hsu AY, Ghimire L, et al. 2024. The palmitoylation of gasdermin D directs its membrane translocation and pore formation during pyroptosis. *Science Immunology*, **9**(94): eadn1452.

Bijlmakers MJ, Marsh M. 2003. The on–off story of protein palmitoylation. *Trends in Cell Biology*, **13**(1): 32–42.

Blewett TA, Binning SA, Weinrauch AM, et al. 2022. Physiological and behavioural strategies of aquatic animals living in fluctuating environments. *Journal of Experimental Biology*, **225**(9): jeb242503.

Boehm T, Swann JB. 2014. Origin and evolution of adaptive immunity. *Annual Review of Animal Biosciences*, **2**(1): 259–283.

Chen BH, Zhou ZX, Ke QZ, et al. 2019. The sequencing and *de novo* assembly of the *Larimichthys crocea* genome using PacBio and Hi-C technologies. *Scientific Data*, **6**(1): 188.

Chen H, Ding SF, Tan JC, et al. 2020. Characterization of the Japanese flounder NLRP3 inflammasome in restricting *Edwardsiella piscicida* colonization *in vivo*. *Fish & Shellfish Immunology*, **103**: 169–180.

Chen JQ, Chen ZJ. 2018. PtdIns4P on dispersed *trans*-Golgi network mediates NLRP3 inflammasome activation. *Nature*, **564**(7734): 71–76.

Chen SW, Jin P, Chen H, et al. 2021. Dual function of a turbot inflammatory caspase in mediating both canonical and non-canonical inflammasome activation. *Developmental & Comparative Immunology*, **121**: 104078.

Chuphal B, Rai U, Roy B. 2022. Teleost NOD-like receptors and their downstream signaling pathways: a brief review. *Fish and Shellfish Immunology Reports*, **3**: 100056.

Dai T, Zhao ZY, Zhu TF, et al. 2024. The anti-inflammatory role of zDHHC23 through the promotion of macrophage M2 polarization and macrophage necroptosis in large yellow croaker (*Larimichthys crocea*).

Frontiers in Immunology, **15**: 1401626.
Drisdel RC, Alexander JK, Sayeed A, et al. 2006. Assays of protein palmitoylation. *Methods*, **40**(2): 127–134.
Franchi L, Eigenbrod T, Muñoz-Planillo R, et al. 2009. The inflammasome: a caspase-1-activation platform that regulates immune responses and disease pathogenesis. *Nature Immunology*, **10**(3): 241–247.
He Y, Hara H, Núñez G. 2016a. Mechanism and regulation of NLRP3 inflammasome activation. *Trends in Biochemical Sciences*, **41**(12): 1012–1021.
He Y, Zeng MY, Yang DH, et al. 2016b. NEK7 is an essential mediator of NLRP3 activation downstream of potassium efflux. *Nature*, **530**(7590): 354–357.
Holbrook JA, Jarosz-Griffiths HH, Caseley E, et al. 2021. Neurodegenerative disease and the NLRP3 inflammasome. *Frontiers in Pharmacology*, **12**: 643254.
Hu DW, Li YT, Wang XY, et al. 2024. Palmitoylation of NLRP3 modulates inflammasome activation and inflammatory bowel disease development. *The Journal of Immunology*, **213**(4): 481–493.
Huang L, Zhao L, Su Y, et al. 2018. Genome sequence of *Pseudomonas plecoglossicida* strain NZBD9. *Genome Announcements*, **6**(4): e01412–17.
Kon T, Pei LY, Ichikawa R, et al. 2021. Whole-genome resequencing of large yellow croaker (*Larimichthys crocea*) reveals the population structure and signatures of environmental adaptation. *Scientific Reports*, **11**(1): 11235.
Lemonidis K, Werno MW, Greaves J, et al. 2015. The zDHHC family of S-acyltransferases. *Biochemical Society Transactions*, **43**(2): 217–221.
Li CH, Chen J, Nie L, et al. 2020a. MOSPD2 is a receptor mediating the LEAP-2 effect on monocytes/macrophages in a teleost, *Boleophthalmus pectinirostris*. *Zoological Research*, **41**(6): 644–655.
Li JY, Wang YY, Shao T, et al. 2020b. The zebrafish NLRP3 inflammasome has functional roles in ASC-dependent interleukin-1β maturation and gasdermin E-mediated pyroptosis. *Journal of Biological Chemistry*, **295**(4): 1120–1141.
Mangan MSJ, Olhava EJ, Roush WR, et al. 2018. Targeting the NLRP3 inflammasome in inflammatory diseases. *Nature Reviews Drug Discovery*, **17**(8): 588–606.
Martinon F, Burns K, Tschopp J. 2002. The inflammasome: a molecular platform triggering activation of inflammatory caspases and processing of proIL-beta. *Molecular Cell*, **10**(2): 417–426.
Nie L, Fei CJ, Fan YZ, et al. 2024. Consecutive palmitoylation and phosphorylation orchestrates NLRP3 membrane trafficking and inflammasome activation. *Molecular Cell*, **84**(17): 3336–3353. e7.
Rocks O, Gerauer M, Vartak N, et al. 2010. The palmitoylation machinery is a spatially organizing system for peripheral membrane proteins. *Cell*, **141**(3): 458–471.
Sharma BR, Kanneganti TD. 2021. NLRP3 inflammasome in cancer and metabolic diseases. *Nature Immunology*, **22**(5): 550–559.
Shi HX, Murray A, Beutler B, 2016. Reconstruction of the mouse inflammasome system in HEK293T cells. *Bio-protocol*, **6**(21): e1986.
Shi JJ, Zhao Y, Wang K, et al. 2015. Cleavage of GSDMD by inflammatory caspases determines pyroptotic cell death. *Nature*, **526**(7575): 660–665.
Sun YJ, Nie P, Zhao LM, et al. 2019. Dual RNA-Seq unveils the role of the *Pseudomonas plecoglossicida fliA* gene in pathogen-host interaction with *Larimichthys crocea*. *Microorganisms*, **7**(10): 443.
Tan MS, Yu JT, Jiang T, et al. 2013. The NLRP3 inflammasome in Alzheimer's disease. *Molecular Neurobiology*, **48**(3): 875–882.
Tang Y, Xin G, Zhao LM, et al. 2020. Novel insights into host-pathogen interactions of large yellow croakers (*Larimichthys crocea*) and pathogenic bacterium *Pseudomonas plecoglossicida* using time-resolved dual RNA-seq of infected spleens. *Zoological Research*, **41**(3): 314–327.
Tao Z, Xu Y, Zhou SM, et al. 2020. Acquisition of a type VI secretion system is critical for *Pseudomonas plecoglossicida* induced granulomas in fish internal organs. *Aquaculture*, **516**: 734629.
Wang LQ, Cai J, Zhao X, et al. 2023. Palmitoylation prevents sustained inflammation by limiting NLRP3 inflammasome activation through chaperone-mediated autophagy. *Molecular Cell*, **83**(2): 281–297. e10.
Wu CW, Zhang D, Kan MY, et al. 2014. The draft genome of the large yellow croaker reveals well-developed innate immunity. *Nature Communications*, **5**(1): 5227.
Wu XY, Xiong JB, Fei CJ, et al. 2022. Prior exposure to ciprofloxacin disrupts intestinal homeostasis and predisposes ayu (*Plecoglossus altivelis*) to subsequent *Pseudomonas plecoglossicida*-induced infection. *Zoological Research*, **43**(4): 648–665.
Yu T, Hou D, Zhao JQ, et al. 2024. NLRP3 Cys126 palmitoylation by ZDHHC7 promotes inflammasome activation. *Cell Reports*, **43**(4): 114070.
Yuan B, Zhao LM, Zhuang ZX, et al. 2022. Transcriptomic and metabolomic insights into the role of the *flgK* gene in the pathogenicity of *Pseudomonas plecoglossicida* to orange-spotted grouper (*Epinephelus coioides*). *Zoological Research*, **43**(6): 952–965.
Zheng SH, Que XY, Wang SX, et al. 2023. ZDHHC5-mediated NLRP3 palmitoylation promotes NLRP3-NEK7 interaction and inflammasome activation. *Molecular Cell*, **83**(24): 4570–4585. e7.
Zhou Y, Tong ZZ, Jiang SH, et al. 2020. The roles of *Endoplasmic Reticulum* in NLRP3 inflammasome activation. *Cells*, **9**(5): 1219.